Applied Optics, Volume 59, Issue 25, 2020, pp. 7694-7704
DOI:10.1364/AO.396922

Polarization-sensitive transfer matrix modelling fo rdisplacement measuring interferometry

Angus Bridges[1,2], Andrew Yacoot[1], Thomas Kissinger[2], and Ralph P. Tatam[2,*]

[1]National Physical Laboratory, Teddington, Middlesex, TW11 0LW, United Kingdom
[2]Centre for Engineering Photonics, Cranfield University, MK43 0AL, United Kingdom
[*]Corresponding author: r.p.tatam@cranfield.ac.uk

The use of polarising optics both for beam steering and phase measurement applications in displacement measuring interferometer designs is almost universal. Interferometer designs that employ polarising optics in this manner are particularly sensitive to the effects of unwanted optical cavities that form within the optics due to polarisation leakage and back reflections from material interfaces. Modelling techniques commonly employed in the design of such interferometers are poorly suited to the analysis of multiple passes through polarising optics. A technique, along with an accompanying software implementation, is presented here that is capable of modelling the propagation of monochromatic plane waves through an arbitrary network of linear planar optical components.

1 Introduction

Displacement measuring optical interferometers are widely employed where displacement measurements that are traceable back to the realisation and definition of the SI metre [1, 2] with nanometre or sub-nanometre resolution are required, either directly or via the calibration of other instruments [3]. Such interferometers suffer from non-linearities, errors in the measured displacement that are periodic with the wavelength of the illuminating light, introduced by a variety of sources [4], many of which can be corrected using a Heydemann style ellipse fitting correction [5, 6]. Non-linearities that cannot be corrected with currently available techniques are introduced by the formation of weakly resonant cavities within the optics of interferometer designs [7].

Complex networks of interconnected cavities may be introduced either by back reflections at material interfaces, or by polarisation leakage in polarising beam splitters, combined with imperfections in other polarising optics. Many displacement measuring interferometer designs [8, 9, 4, 10, 11, 12, 13, 14, 15, 16, 17] include polarising beam splitters, and such designs are particularly vulnerable to multiple pass effects due to the combined contributions of polarisation leakage and unwanted back reflections. Polarisation aberrations can be particularly complex to analyse, as they may be introduced not only by imperfections in the polarising optics but also by reflections, often from multi-layer or metallic optical coatings, at non-normal angles of incidence, for example within corner cube retro-reflectors [18].

Modelling the effects of these complex networks of cavities with existing techniques commonly employed for interferometer design can be challenging. Jones calculus [19, 20, 21, 22, 23, 24, 25], for example, is often applied to modelling optical systems made up of planar polarising optics. Jones calculus models polarising optics by propagating a unidirectional electrical plane wave through a defined series of optical components. Due to this unidirectional treatment all possible optical paths must be modelled separately, with the final electric field amplitudes being combined to determine the outputs of an optical network. For optical networks containing many interconnected cavities tracing all possible optical paths is an error prone process, and multiple passes must be handled iteratively, with some cut off imposed. An alternative technique is employed by the FINESSE software [26, 27], aimed primarily at gravitation wave detector design where optical cavities are a desired feature [28], in which the optical network is considered as a network of nodes, with counter-propagating electric fields coupled together at each node in a similar manor to that employed in thin film transfer matrix modelling techniques [29]. This approach is better suited to the assessment of networks of interconnected cavities (both intentional and unintentional in nature), however the FINESSE software does not account for the effects of polarising optics, and cannot model the effects of reflection from or transmission through optically absorbing materials or coatings. As a result of these limitations FINESSE is of limited applicability to displacement measuring interferometer design. Alternative approaches to modelling the effects of multiple passes through optical networks include finite element analysis and ray tracing [30, 31] models. Finite element analysis requires a careful mesh design and even then can be impractically computationally intensive as nanoscale resolutions are required over the macroscopic size of the optics to be modelled. Ray tracing approaches must be iterated many times to take into account the effect of cavity formation, and may not produce reliable results, with the effects of cavities of various strengths and optical path lengths being artificially amplified relative to each other depending on the cut-off point imposed on ray propagation. Both ray tracing and finite element analysis approaches require a model of the morphology of the optical components

Published by OSA. This is the Author Accepted Manuscript issued with: Creative Commons Attribution Non-Commercial License (CC:BY:NC 4.0).
The final published version (version of record) is available online at DOI:10.1364/AO.396922. Please refer to any applicable publisher terms of use.

to be constructed, rather than dealing with a relatively simple list of optical components as is the case for Jones calculus and FINESSE. Whilst further complexity is added to the model, defining the morphology of the optical components does give finite element analysis and ray tracing techniques the advantage that free-form optical surfaces can be modelled, and finite element techniques have the additional advantage of being able to model diffraction effects.

A modelling technique is presented here that aims to allow the effects of the formation of weakly resonant cavities within networks of planar optical surfaces to be analysed. This approach extends the transfer matrix methodology commonly applied to thin film modelling [32, 33, 29] to model multiple port devices and the effects of polarisation, combining transfer and scattering matrices to describe an optical network in a manner similar to that of the FINESSE software [26]. This allows the bidirectional propagation of polarised light to be modelled, along with the effects of reflection from and transmission through absorbing (metallic) materials. This is achieved by coupling together pairs of counter-propagating electrical plane waves at nodes in an optical network. By modelling coupled networks of polarising optical components in this way, the effects of polarisation aberrations and unwanted back reflections within the optics of displacement measuring interferometers can be assessed, and used to inform improved interferometer designs. A software implementation of this modelling technique is available [34].

2 Theory

The methodology presented here describes a system of optical components with a network of interconnected nodes, with a node at each input/output port of individual optical components, as is done in the FINESSE software [26]. A complex valued electric field is defined as the sum of two counter-propagating complex valued electrical plane waves travelling along the positive and negative $\hat{\boldsymbol{z}}$ direction [29] at each node n, where $\hat{\boldsymbol{z}}$ is the unit vector in the positive z direction, as

$$\boldsymbol{E}_n = \boldsymbol{A}_F e^{i(kz-\omega t+\varphi)} + \boldsymbol{A}_B e^{i(-kz-\omega t+\varphi)} \tag{1}$$

where $\boldsymbol{A}_F$ and $\boldsymbol{A}_B$ are the complex amplitudes of the forward and backward propagating components, k is the wavenumber, ω is the angular frequency, t is time and φ is a phase offset. The physical potential of the electrical field at a given time is given by the real component of equation 1. These forward and backward propagating components can be further decomposed into orthogonally polarised (along the $\hat{\boldsymbol{x}}$ and $\hat{\boldsymbol{y}}$ directions) counter-propagating components

$$E_{F,x,n} = A_{F,x} e^{i(kz-\omega t+\varphi)}, \tag{2}$$
$$E_{F,y,n} = A_{F,y} e^{i(kz-\omega t+\varphi)}, \tag{3}$$
$$E_{B,x,n} = A_{B,x} e^{i(-kz-\omega t+\varphi)}, \tag{4}$$
$$E_{B,y,n} = A_{B,y} e^{i(-kz-\omega t+\varphi)}. \tag{5}$$

By making the assumption that we are interested only in steady state (on timescales of the speed of light) solutions, the temporal component of equations 2 to 5 may be neglected, as any steady state solution must be valid at time zero. The choice of absolute phase is also arbitrary in this case, allowing the phase offset φ to be set to zero. For a given steady state solution the spatial position of each node n is constant, allowing the remaining exponential term to be absorbed into the complex amplitude. A coordinate system may then be chosen such that polarisation components along the $\hat{\boldsymbol{x}}$ and $\hat{\boldsymbol{y}}$ directions represent S and P polarisation states for any material boundaries at node n, and the 'forward' and 'backward' components may be denoted as a and b components of the electric field for the sake of brevity of notation. Equations 2 to 5 can then be rewritten as

$$a_n^{(\mathrm{S})} = E_{F,x,n}, \tag{6}$$
$$a_n^{(\mathrm{P})} = E_{F,y,n}, \tag{7}$$
$$b_n^{(\mathrm{S})} = E_{B,x,n}, \tag{8}$$
$$b_n^{(\mathrm{P})} = E_{B,y,n}. \tag{9}$$

The choice of S and P basis states is made for convenience, an arbitrary polarisation state may be decomposed into any orthogonal pair of basis states, and in some cases left and right hand circularly polarised states may be preferable.

These assumptions along with the choice of coordinate system have several important consequences to the application of the modelling technique. Firstly, by considering only plane wave forms, all optical interfaces are taken to be planar and infinite in extent. As such the effects of diffraction [35] and wavefront curvature [36] cannot be modelled. Secondly by neglecting the temporal component, the model is restricted to monochromatic light, although the results may be readily applied to physical quasi-monochromatic light [37]. An additional result of the plane wave assumption is that all beams are also assumed to be infinite in extent, and as such losses due to misalignment and higher order multiple passes 'missing' detectors cannot be modelled. Finally, in order to maintain the physical meaning of the S and P polarised components, changes of coordinate system must take place between optical components where the S and P polarisation states of the material interface planes do not align.

In order to model networks of optical components, the electric field components defined at each node must be linked together. This is achieved in this modelling methodology with a series of scattering and transfer matrix equations. The system of linear equations formed by these scattering and transfer matrix equations is then rewritten in the form of a single network matrix equation, which can be solved to find the values of the electric field components for a given set of boundary conditions.

A scattering matrix is defined here as a matrix linking all outputs of an optical device to all inputs to the same device, which may be generalised to optical devices with any number of ports. A port refers to an input or output of a device; for example, a planar interface between two materials with light normally incident is a two port device and a freespace beam splitter is a four port device. A device with a port number N_p is described by an $2N_p \times 2N_p$ scattering matrix $\boldsymbol{S}$, linking input and output S and P polarised components for each port. As such, the scattering matrix representation of the freespace

beam splitter depicted in figure 1 is

$$\begin{pmatrix} b_0^{(\mathrm{S})} \\ b_0^{(\mathrm{P})} \\ b_1^{(\mathrm{S})} \\ b_1^{(\mathrm{P})} \\ b_2^{(\mathrm{S})} \\ b_2^{(\mathrm{P})} \\ b_3^{(\mathrm{S})} \\ b_3^{(\mathrm{P})} \end{pmatrix} = \boldsymbol{S} \begin{pmatrix} a_0^{(\mathrm{S})} \\ a_0^{(\mathrm{P})} \\ a_1^{(\mathrm{S})} \\ a_1^{(\mathrm{P})} \\ a_2^{(\mathrm{S})} \\ a_2^{(\mathrm{P})} \\ a_3^{(\mathrm{S})} \\ a_3^{(\mathrm{P})} \end{pmatrix}, \tag{10}$$

where $\boldsymbol{S}$ is an 8×8 scattering matrix, and the components $a_i^{(\mathrm{S})}$, $a_i^{(\mathrm{P})}$, $b_i^{(\mathrm{S})}$ and $b_i^{(\mathrm{P})}$ represent the S and P polarised input and output fields respectively, at the i^{th} port.

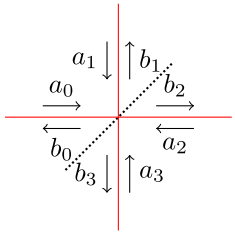

Figure 1: Schematic of the electric field components at a four port beam splitter.

Figure 2: Schematic of the electric field components across two plane parallel interfaces.

Transfer matrices, in contrast to the previously described scattering matrices, are limited to two port devices. A transfer matrix is defined here as the matrix which links the incident and excident fields $a_i^{(\mathrm{S})}$, $a_i^{(\mathrm{P})}$, $b_i^{(\mathrm{S})}$ and $b_i^{(\mathrm{P})}$ at one port of a two port device to the equivalent fields $a_j^{(\mathrm{S})}$, $a_j^{(\mathrm{P})}$, $b_j^{(\mathrm{S})}$ and $b_j^{(\mathrm{P})}$ at the second port. Transfer matrix modelling is a commonly employed technique for multilayer thin film design [29, 33], with transfer matrices used to describe interfaces between materials and propagation matrices to link field components across a single material. For the interfaces depicted in figure 2 transfer matrices link the field components through the equations

$$\begin{pmatrix} a_4^{(\mathrm{S})} \\ a_4^{(\mathrm{P})} \\ b_4^{(\mathrm{S})} \\ b_4^{(\mathrm{P})} \end{pmatrix} = \boldsymbol{T}_{4,5} \begin{pmatrix} a_5^{(\mathrm{S})} \\ a_5^{(\mathrm{P})} \\ b_5^{(\mathrm{S})} \\ b_5^{(\mathrm{P})} \end{pmatrix} \tag{11}$$

and

$$\begin{pmatrix} a_6^{(\mathrm{S})} \\ a_6^{(\mathrm{P})} \\ b_6^{(\mathrm{S})} \\ b_6^{(\mathrm{P})} \end{pmatrix} = \boldsymbol{T}_{6,7} \begin{pmatrix} a_7^{(\mathrm{S})} \\ a_7^{(\mathrm{P})} \\ b_7^{(\mathrm{S})} \\ b_7^{(\mathrm{P})} \end{pmatrix}. \tag{12}$$

A special case of the transfer matrix, the propagation matrix, describes the field on either side of a region made up of a single material with no interfaces. In figure 2 a propagation matrix $\boldsymbol{P}$ links the field amplitudes a_5 and b_5 with a_6 and b_6 as

$$\begin{pmatrix} a_6^{(\mathrm{S})} \\ a_6^{(\mathrm{P})} \\ b_6^{(\mathrm{S})} \\ b_6^{(\mathrm{P})} \end{pmatrix} = \boldsymbol{P}_{5,6} \begin{pmatrix} a_5^{(\mathrm{S})} \\ a_5^{(\mathrm{P})} \\ b_5^{(\mathrm{S})} \\ b_5^{(\mathrm{P})} \end{pmatrix}. \tag{13}$$

Given a set of plane parallel interfaces a global transfer matrix may be calculated from a series of transfer and propagation matrices, relating the incident and excident field amplitudes at each side of the stack of layers. As such the field components $a_4^{(\mathrm{S})}$, $a_4^{(\mathrm{P})}$, $b_4^{(\mathrm{S})}$ and $b_4^{(\mathrm{P})}$ may be linked to $a_7^{(\mathrm{S})}$, $a_7^{(\mathrm{P})}$, $b_7^{(\mathrm{S})}$ and $b_7^{(\mathrm{P})}$ in figure 2 by a global transfer matrix $\boldsymbol{M}$ as

$$\begin{pmatrix} a_4^{(\mathrm{S})} \\ a_4^{(\mathrm{P})} \\ b_4^{(\mathrm{S})} \\ b_4^{(\mathrm{P})} \end{pmatrix} = \boldsymbol{M}_{4,7} \begin{pmatrix} a_7^{(\mathrm{S})} \\ a_7^{(\mathrm{P})} \\ b_7^{(\mathrm{S})} \\ b_7^{(\mathrm{P})} \end{pmatrix}, \tag{14}$$

$$= \boldsymbol{T}_{4,5}\boldsymbol{P}_{5,6}\boldsymbol{T}_{6,7} \begin{pmatrix} a_7^{(\mathrm{S})} \\ a_7^{(\mathrm{P})} \\ b_7^{(\mathrm{S})} \\ b_7^{(\mathrm{P})} \end{pmatrix}. \tag{15}$$

The forms of the matrices in equations 11 to 13 are described in the following section, and a more detailed treatment of this widely employed technique as applied to a 2×2 single polarisation state system can be found in the literature [29].

A set of scattering and transfer matrix equations linking together a network of nodes, together with equations defining the inputs to the network, form a set of linear equations that may be written as a single matrix equation. By solving this system using standard numerical techniques the values of the electric fields at various points within the network may be found.

3 Modelling examples

3.1 Matrices of common optical components

The transfer or scattering matrices for a range of optical components commonly employed in interferometry are presented here in order to demonstrate the utility of the modelling methodology. This selection of optical components is sufficient to model a wide range of optical systems, however it is not an exhaustive list, and the technique is widely applicable to modelling linear optical components. All optical components described here are available in the accompanying software implementation [34].

3.1.1 Free space propagation

The simplest possible transfer matrix describes the propagation of light through free space. For propagation between node 0 and node 1 the transfer matrix equation is given by

$$\begin{pmatrix} a_1^{(\mathrm{P})} \\ b_1^{(\mathrm{P})} \\ a_1^{(\mathrm{S})} \\ b_1^{(\mathrm{S})} \end{pmatrix} = \begin{pmatrix} e^{ik_z d} & 0 & 0 & 0 \\ 0 & e^{-ik_z d} & 0 & 0 \\ 0 & 0 & e^{ik_z d} & 0 \\ 0 & 0 & 0 & e^{-ik_z d} \end{pmatrix} \begin{pmatrix} a_0^{(\mathrm{P})} \\ b_0^{(\mathrm{P})} \\ a_0^{(\mathrm{S})} \\ b_0^{(\mathrm{S})} \end{pmatrix}, \tag{16}$$

where k_z is the component of the wavevector normal to the optical interface planes and d is the distance between the interfaces. The above equation assumes an optically homogeneous and isotropic medium, propagation in birefringent media will introduce non-diagonal terms into the propagation matrix. For absorbing media the wavevector will be complex valued, and hence introduce an exponential amplitude decay with propagation distance as expected for negative imaginary components of the complex index when following the sign conventions in this work.

3.1.2 Material interface

The interface between two materials may also be represented as a transfer matrix. Extending the transfer matrix formalism commonly employed in thin film modelling [29] to handle both S and P polarisations [32, 38, 39], the transfer matrix equation from the zeroth to the first node may be written in terms of the S and P polarised amplitude reflection and transmission coefficients $r^{(\mathrm{S})}$, $r^{(\mathrm{P})}$, $t^{(\mathrm{S})}$ and $t^{(\mathrm{P})}$ as

$$\begin{pmatrix} a_1^{(\mathrm{P})} \\ b_1^{(\mathrm{P})} \\ a_1^{(\mathrm{S})} \\ b_1^{(\mathrm{S})} \end{pmatrix} = \begin{pmatrix} \frac{1}{t^{(\mathrm{P})}} & \frac{r^{(\mathrm{P})}}{t^{(\mathrm{P})}} & 0 & 0 \\ \frac{r^{(\mathrm{P})}}{t^{(\mathrm{P})}} & \frac{1}{t^{(\mathrm{P})}} & 0 & 0 \\ 0 & 0 & \frac{1}{t^{(\mathrm{S})}} & \frac{r^{(\mathrm{S})}}{t^{(\mathrm{S})}} \\ 0 & 0 & \frac{r^{(\mathrm{S})}}{t^{(\mathrm{S})}} & \frac{1}{t^{(\mathrm{S})}} \end{pmatrix} \begin{pmatrix} a_0^{(\mathrm{P})} \\ b_0^{(\mathrm{P})} \\ a_0^{(\mathrm{S})} \\ b_0^{(\mathrm{S})} \end{pmatrix}. \tag{17}$$

This transfer matrix may be used in combination with the previously described transfer matrix for free space propagation to construct optical paths passing through several materials, and by taking the product of several such matrices propagation through multiple layers of materials may be modelled with a single transfer matrix [29]. As for the previously described propagation matrix, birefringent materials will introduce additional polarisation mixing terms into the transfer matrix. If light at non-normal angles of incidence is to be modelled, the effects of the infinite plane wave assumption must be considered; for layers separated by microscopic distances this is unlikely to present a problem, however if layers with macroscopic thicknesses are to be modelled, it should be noted that at non-normal angles of incidence the reflected beams will not be lost. Care must also be taken with the calculation of the amplitude transmission and reflection coefficients if absorbing materials are to be included where for propagation through a single material interface from material $m-1$ to m the coefficients are given by

$$r_{m-1,m}^{(\mathrm{P})} = \frac{\tilde{n}_{m-1}^2 k_{z,m} - \tilde{n}_m^2 k_{z,m-1}}{\tilde{n}_{m-1}^2 k_{z,m} + \tilde{n}_m^2 k_{z,m-1}}, \tag{18}$$

$$t_{m-1,m}^{(\mathrm{P})} = \frac{\tilde{n}_{m-1}}{\tilde{n}_m} \left(1 + r_{m-1,m}\right), \tag{19}$$

$$r_{m-1,m}^{(\mathrm{S})} = \frac{k_{z,m-1} - k_{z,m}}{k_{z,m-1} + k_{z,m}} \tag{20}$$

and

$$t_{m-1,m}^{(\mathrm{S})} = 1 + r_{m-1,m}, \tag{21}$$

$$= \frac{2k_{z,m-1}}{k_{z,m-1} + k_{z,m}}, \tag{22}$$

where $\tilde{n}_m$ is the complex refractive index in material m and $k_{z,m}$ is the component of the wavevector normal to the interface in material m. This wavevector form of the Fresnel coefficients may be derived by applying trigonometry to the standard derivation of the Fresnel coefficients [40], and avoids calculations involving non-physical complex propagation angles introduced by the difference in propagation direction of planes of constant phase and amplitude in absorbing media [41]. For propagation through multiple parallel layers calculation of these coefficients can be simplified by taking advantage of the fact that the component of the wavevector that is parallel to the material interface planes remains constant throughout, allowing the normal component of the wavevector in material m to be calculated from

$$k_{z,m} = \sqrt{\left(\frac{2\pi\tilde{n}}{\lambda_0}\right)^2 - k_{\shortparallel}^2}, \tag{23}$$

in a non-absorbing material where $k_{\shortparallel}$ is the parallel component of the wavevector in all layers.

3.1.3 Linear polariser

A non-ideal linear polariser is described here by three properties: rotation angle (θ), extinction coefficient (ρ) and loss (α). The rotation angle here is measured clockwise from the S polarised axis looking from the zeroth node to the first although the physical meaning of this rotation will depend on the orientation in which the scattering matrix is coupled into the optical network. The extinction coefficient is defined as the intensity ratio of transmitted light polarised perpendicular to the transmission axis of the polariser, to the intensity of transmitted light polarised parallel to the transmission axis. Loss is similarly defined as the intensity ratio of transmitted light polarised parallel to the transmission axis to the intensity of the component of the incident light polarised along that axis. As such an ideal polariser has an extinction coefficient and loss of zero.

Whilst a linear polariser is a two port device, it is more readily represented as a scattering matrix. Using the above definitions the scattering matrix equation of a polariser aligned to the S polarisation axis is given by

$$\begin{aligned} \begin{pmatrix} b_0^{(\mathrm{P})} \\ b_0^{(\mathrm{S})} \\ b_1^{(\mathrm{P})} \\ b_1^{(\mathrm{S})} \end{pmatrix} &= \begin{pmatrix} 0 & 0 & \sqrt{\rho(1-\alpha)} & 0 \\ 0 & 0 & 0 & \sqrt{1-\alpha} \\ \sqrt{\rho(1-\alpha)} & 0 & 0 & 0 \\ 0 & \sqrt{1-\alpha} & 0 & 0 \end{pmatrix} \begin{pmatrix} a_0^{(\mathrm{P})} \\ a_0^{(\mathrm{S})} \\ a_1^{(\mathrm{P})} \\ a_1^{(\mathrm{S})} \end{pmatrix}, \\ &= \boldsymbol{S}_{\mathrm{POL}}^{(\mathrm{S})} \begin{pmatrix} a_0^{(\mathrm{P})} \\ a_0^{(\mathrm{S})} \\ a_1^{(\mathrm{P})} \\ a_1^{(\mathrm{S})} \end{pmatrix}. \end{aligned} \tag{24}$$

The scattering matrix of a rotated polariser may be found by applying the rotation matrix

$$\boldsymbol{R}(\theta) = \begin{pmatrix} \cos(\theta) & -\sin(\theta) & 0 & 0 \\ \sin(\theta) & \cos(\theta) & 0 & 0 \\ 0 & 0 & \cos(\theta) & -\sin(\theta) \\ 0 & 0 & \sin(\theta) & \cos(\theta) \end{pmatrix}, \tag{25}$$

to the vector of incident field components, effectively a rotation of the coordinate frame, then rotating back into the frame of the model. As such the scattering matrix of a rotated polariser is given by

$$\boldsymbol{S}_{\mathrm{POL}}^{(\theta)} = \boldsymbol{R}(-\theta)\boldsymbol{S}_{\mathrm{POL}}^{(\mathrm{S})}\boldsymbol{R}(\theta). \tag{26}$$

3.1.4 Waveplate

A waveplate introducing a phase difference η between the S and P polarised beams, orientated with the fast axis along the S polarised direction may be represented by the scattering matrix equation

$$\begin{pmatrix} b_0^{(\mathrm{P})} \\ b_0^{(\mathrm{S})} \\ b_1^{(\mathrm{P})} \\ b_1^{(\mathrm{S})} \end{pmatrix} = \begin{pmatrix} 0 & 0 & e^{-\frac{i\eta}{2}} & 0 \\ 0 & 0 & 0 & e^{\frac{i\eta}{2}} \\ e^{-\frac{i\eta}{2}} & 0 & 0 & 0 \\ 0 & e^{\frac{i\eta}{2}} & 0 & 0 \end{pmatrix} \begin{pmatrix} a_0^{(\mathrm{P})} \\ a_0^{(\mathrm{S})} \\ a_1^{(\mathrm{P})} \\ a_1^{(\mathrm{S})} \end{pmatrix}, \\ = \boldsymbol{S}_{\mathrm{WP}}^{(\mathrm{S})} \begin{pmatrix} a_0^{(\mathrm{P})} \\ a_0^{(\mathrm{S})} \\ a_1^{(\mathrm{P})} \\ a_1^{(\mathrm{S})} \end{pmatrix}. \quad (27)$$

This matrix can be seen to be closely related to the corresponding Jones matrix for an optical retarder [19], and Jones matrices can in general be easily rewritten as scattering matrices. In the same manner as previously discussed for a linear polariser, the scattering matrix of a rotated waveplate is given by

$$\boldsymbol{S}_{\mathrm{WP}}^{(\theta)} = \boldsymbol{R}(-\theta)\boldsymbol{S}_{\mathrm{WP}}^{(\mathrm{S})}\boldsymbol{R}(\theta), \quad (28)$$

where rotation is again measured clockwise from the S polarised axis looking from the zeroth node to the first.

3.1.5 Faraday rotator

Faraday rotators are commonly employed as optical isolators. Whilst the scattering matrix of an ideal optical isolator could be defined trivially, in some cases it may be of interest to model the effects of multiple reflections through a non-ideal isolator. Such a device may be modelled using the previously described equations for a linear polariser, in combination with a Faraday rotator.

The scattering matrix of a Faraday rotator with loss α as previously defined is given by

$$\boldsymbol{S}_{\mathrm{FR}}^{(\psi)} = \sqrt{1-\alpha} \begin{pmatrix} 0 & 0 & \cos(\psi) & -\sin(\psi) \\ 0 & 0 & \sin(\psi) & \cos(\psi) \\ \cos(\psi) & -\sin(\psi) & 0 & 0 \\ \sin(\psi) & \cos(\psi) & 0 & 0 \end{pmatrix}, \quad (29)$$

where ψ is the angle of the polarisation rotation introduced by the polariser, with rotation measured clockwise looking from the zeroth node to the first.

3.1.6 Non-polarising beam splitter

The properties of an ideal lossless non-polarising beam splitter may be defined by the ratio of reflected intensity to transmitted intensity, ζ. For a set value of ζ, the amplitude reflectivity r and transmission t coefficients are given by

$$r = \sqrt{\frac{\zeta}{\zeta+1}} \quad (30)$$

and

$$t = \sqrt{\frac{1}{\zeta+1}}. \quad (31)$$

Referring back to figure 1, the scattering matrix equation linking the four nodes is given by

$$\begin{pmatrix} b_0^{(\mathrm{P})} \\ b_0^{(\mathrm{S})} \\ b_1^{(\mathrm{P})} \\ b_1^{(\mathrm{S})} \\ b_2^{(\mathrm{P})} \\ b_2^{(\mathrm{S})} \\ b_3^{(\mathrm{P})} \\ b_3^{(\mathrm{S})} \end{pmatrix} = \begin{pmatrix} 0 & 0 & r & 0 & t & 0 & 0 & 0 \\ 0 & 0 & 0 & r & 0 & t & 0 & 0 \\ r & 0 & 0 & 0 & 0 & 0 & t & 0 \\ 0 & r & 0 & 0 & 0 & 0 & 0 & t \\ t & 0 & 0 & 0 & 0 & 0 & r & 0 \\ 0 & t & 0 & 0 & 0 & 0 & 0 & r \\ 0 & 0 & t & 0 & r & 0 & 0 & 0 \\ 0 & 0 & 0 & t & 0 & r & 0 & 0 \end{pmatrix} \begin{pmatrix} a_0^{(\mathrm{P})} \\ a_0^{(\mathrm{S})} \\ a_1^{(\mathrm{P})} \\ a_1^{(\mathrm{S})} \\ a_2^{(\mathrm{P})} \\ a_2^{(\mathrm{S})} \\ a_3^{(\mathrm{P})} \\ a_3^{(\mathrm{S})} \end{pmatrix}. \quad (32)$$

From this equation it is clear that the coupling between individual nodes and polarisations can be readily changed. Realistic beam splitter coatings can be modelled if desired by calculating the amplitude reflection and transmission coefficients for each polarisation (the Fresnel coefficients) using transfer matrix modelling techniques from the layer structure of the beam splitter coating.

3.1.7 Polarising beam splitter

A polarising beam splitter can be defined by a set of coefficients similar to those used previously to define a linear polariser. Extinction coefficients must be defined separately for the reflected and transmitted beams as ρ_{R}, ρ_{T}, and similarly loss coefficients for each polarisation as $\alpha^{(\mathrm{S})}$ and $\alpha^{(\mathrm{P})}$. This distinction is necessary as for commonly available thin film based polarising beam splitters, the extinction coefficient of the reflected beam is often significantly poorer than that of the transmitted beam, due to the reliance on Brewster's angle reflections. A polarising beam splitter aligned such that S polarised light is reflected and P polarised light transmitted may be described with the scattering matrix equation

$$\begin{pmatrix} b_0^{(\mathrm{P})} \\ b_0^{(\mathrm{S})} \\ b_1^{(\mathrm{P})} \\ b_1^{(\mathrm{S})} \\ b_2^{(\mathrm{P})} \\ b_2^{(\mathrm{S})} \\ b_3^{(\mathrm{P})} \\ b_3^{(\mathrm{S})} \end{pmatrix} = \begin{pmatrix} 0 & 0 & r^{(\mathrm{P})} & 0 & t^{(\mathrm{P})} & 0 & 0 & 0 \\ 0 & 0 & 0 & r^{(\mathrm{S})} & 0 & t^{(\mathrm{S})} & 0 & 0 \\ r^{(\mathrm{P})} & 0 & 0 & 0 & 0 & 0 & t^{(\mathrm{P})} & 0 \\ 0 & r^{(\mathrm{S})} & 0 & 0 & 0 & 0 & 0 & t^{(\mathrm{S})} \\ t^{(\mathrm{P})} & 0 & 0 & 0 & 0 & 0 & r^{(\mathrm{P})} & 0 \\ 0 & t^{(\mathrm{S})} & 0 & 0 & 0 & 0 & 0 & r^{(\mathrm{S})} \\ 0 & 0 & t^{(\mathrm{P})} & 0 & r^{(\mathrm{P})} & 0 & 0 & 0 \\ 0 & 0 & 0 & t^{(\mathrm{S})} & 0 & r^{(\mathrm{S})} & 0 & 0 \end{pmatrix} \begin{pmatrix} a_0^{(\mathrm{P})} \\ a_0^{(\mathrm{S})} \\ a_1^{(\mathrm{P})} \\ a_1^{(\mathrm{S})} \\ a_2^{(\mathrm{P})} \\ a_2^{(\mathrm{S})} \\ a_3^{(\mathrm{P})} \\ a_3^{(\mathrm{S})} \end{pmatrix}, \\ = \boldsymbol{S}_{\mathrm{PBS}} \begin{pmatrix} a_0^{(\mathrm{P})} \\ a_0^{(\mathrm{S})} \\ a_1^{(\mathrm{P})} \\ a_1^{(\mathrm{S})} \\ a_2^{(\mathrm{P})} \\ a_2^{(\mathrm{S})} \\ a_3^{(\mathrm{P})} \\ a_3^{(\mathrm{S})} \end{pmatrix}. \quad (33)$$

Defining the reflected and transmitted extinction coefficients as

$$\rho_R = \frac{|r^{(\mathrm{P})}|^2}{|r^{(\mathrm{S})}|^2} \quad (34)$$

and

$$\rho_T = \frac{|t^{(\mathrm{S})}|^2}{|t^{(\mathrm{P})}|^2} \quad (35)$$

and the S and P polarised loss coefficients as

$$\alpha^{(\mathrm{S})} = |r^{(\mathrm{S})}|^2 + |t^{(\mathrm{S})}|^2 \tag{36}$$

and

$$\alpha^{(\mathrm{P})} = |r^{(\mathrm{P})}|^2 + |t^{(\mathrm{P})}|^2 \tag{37}$$

leads to

$$|r^{(\mathrm{S})}|^2 = \frac{\alpha^{(\mathrm{S})} - \alpha^{(\mathrm{P})}\rho_T}{1 - \rho_T\rho_R}, \tag{38}$$

$$|r^{(\mathrm{P})}|^2 = \frac{\rho_R\left(\alpha^{(\mathrm{S})} - \alpha^{(\mathrm{P})}\rho_T\right)}{1 - \rho_T\rho_R}, \tag{39}$$

$$|t^{(\mathrm{S})}|^2 = \frac{\alpha^{(\mathrm{P})}\rho_T - \alpha^{(\mathrm{S})}\rho_T\rho_R}{1 - \rho_T\rho_R} \tag{40}$$

and

$$|t^{(\mathrm{P})}|^2 = \frac{\alpha^{(\mathrm{P})} - \alpha^{(\mathrm{S})}\rho_R}{1 - \rho_T\rho_R}. \tag{41}$$

Some care must be taken to ensure that the intensity reflectivity and transmission coefficients remain physical (in the interval $[0, 1]$) when applying these equations, however for real world values of

$$\alpha^{(\mathrm{P})/(\mathrm{S})} \approx 1 \tag{42}$$

and

$$\rho_{R/T} \approx 0 \tag{43}$$

equations 38 to 41 remain valid.

The polarising beam splitter may be rotated about two axes; the axis of transmission from node zero to node two (θ_0) and the axis of transmission from node one to node three (θ_1). As with previously defined rotation angles, these rotations are defined clockwise from the S polarised axis, looking from the zeroth node to the second, and from the first node to the third. This may be accomplished with the block diagonal 8×8 rotation matrix

$$\boldsymbol{R}(\theta_0, \theta_1) = \begin{pmatrix} \boldsymbol{B}(\theta_0) & 0 & \dots & 0 \\ 0 & \boldsymbol{B}(\theta_1) & \dots & 0 \\ \vdots & \vdots & \boldsymbol{B}(\theta_0) & \vdots \\ 0 & 0 & \dots & \boldsymbol{B}(\theta_1) \end{pmatrix}, \tag{44}$$

where the sub-matrices are given by

$$\boldsymbol{B}(\theta_i) = \begin{pmatrix} \cos(\theta_i) & -\sin(\theta_i) \\ \sin(\theta_i) & \cos(\theta_i)) \end{pmatrix}, \tag{45}$$

such that the scattering matrix of the rotated polarising beam splitter is given by

$$\boldsymbol{S}_{\mathrm{PBS}}^{(\theta_0,\,\theta_1)} = \boldsymbol{R}(-\theta_0, -\theta_1)\boldsymbol{S}_{\mathrm{PBS}}\boldsymbol{R}(\theta_0, \theta_1). \tag{46}$$

3.1.8 Mirror

Mirrors may be modelled in two ways: firstly, by simply setting the incident and excident components to be equal for each polarisation state at a port of another optical component, for example a region of free space propagation. Alternatively, the mirror can be modelled as a material interface, accounting for the lossy properties of metallic mirrors. If this is done, the field amplitude incident on the back surface of the mirror must be fixed, in most practical applications at zero.

3.2 Modelling a polarisation splitting homodyne interferometer

To demonstrate the applications of the model, a homodyne interferometer with polarisation based quadrature fringe counting will be modelled. A schematic of this interferometer is shown in figure 3, with the field pairs at each node (0 through 21) shown.

Light is input into this interferometer polarised at 45° to the vertical axis, and is then split into two arms by a polarising beam splitter (PBS). A double pass through a quarter wave plate (QWP) in each arm then switches the polarisation allowing the previously reflected beam to transmit through the PBS and vice versa. In order to perform directional fringe counting two signals are required with a phase difference between them, ideally of 90° (quadrature). To achieve this, the output of the PBS is split with a non-polarising beam splitter (NPBS). For one output, the polarisations are mixed with a polariser at 45° degrees to the vertical, then detected at photodiode one (PD_1). For the second output (PD_2) a QWP with the fast axis vertical is used before the mixing polariser to introduce a 90° phase difference between the measurement and reference beams.

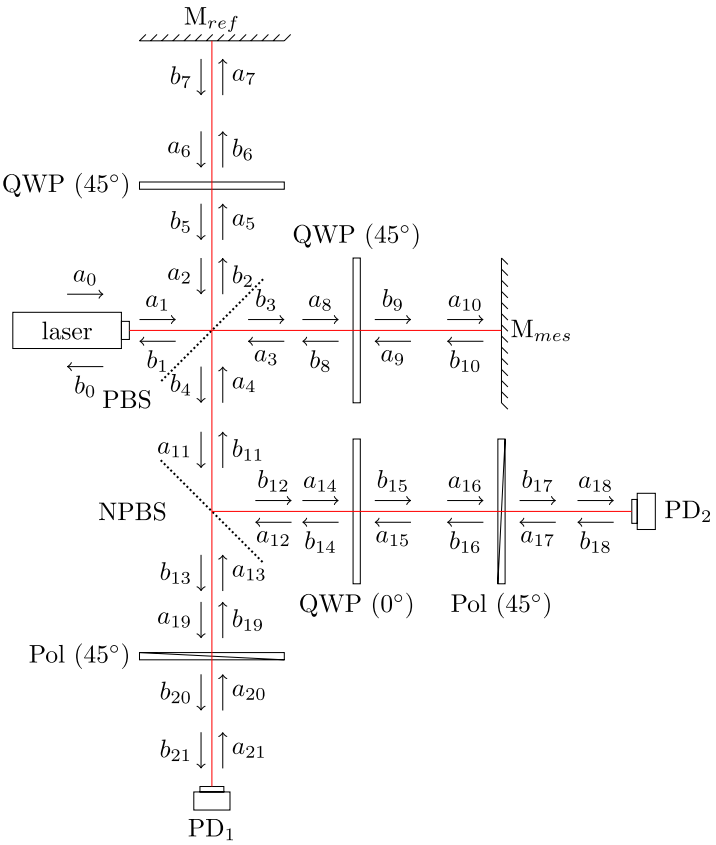

Figure 3: Schematic of the electric field components throughout a homodyne Michelson interferometer with polarising quadrature detection. Counter propagating field components are denoted by a_n and b_n, with the direction of propagation indicated by the corresponding arrows. QWP, quarter wave plate; PBS, polarising beam splitter; NPBS, non-polarising beam splitter; Pol, polariser; PD, photodiode; M$_{ref}$ and M$_{mes}$, reference and measurement mirrors.

The field components may be linked together with transfer and scattering matrices are previously described. For the interferometer depicted in figure 3 the first equation needed is the input, given by

$$\begin{pmatrix} a_0^{(\mathrm{P})} \\ a_0^{(\mathrm{S})} \end{pmatrix} = \begin{pmatrix} \frac{1}{\sqrt{2}} \\ \frac{1}{\sqrt{2}} \end{pmatrix} \tag{47}$$

in the ideal case. The equation of the polarising beam splitter is then given by

$$\begin{pmatrix} b_1^{(\mathrm{P})} \\ b_1^{(\mathrm{S})} \\ b_2^{(\mathrm{P})} \\ b_2^{(\mathrm{S})} \\ b_3^{(\mathrm{P})} \\ b_3^{(\mathrm{S})} \\ b_4^{(\mathrm{P})} \\ b_4^{(\mathrm{S})} \end{pmatrix} = \boldsymbol{S}_{\mathrm{PBS}} \begin{pmatrix} a_1^{(\mathrm{P})} \\ a_1^{(\mathrm{S})} \\ a_2^{(\mathrm{P})} \\ a_2^{(\mathrm{S})} \\ a_3^{(\mathrm{P})} \\ a_3^{(\mathrm{S})} \\ a_4^{(\mathrm{P})} \\ a_4^{(\mathrm{S})} \end{pmatrix}, \tag{48}$$

and the reference arm quarter wave plate by

$$\begin{pmatrix} b_5^{(\mathrm{P})} \\ b_5^{(\mathrm{S})} \\ b_6^{(\mathrm{P})} \\ b_6^{(\mathrm{S})} \end{pmatrix} = \boldsymbol{S}_{\mathrm{WP}}^{(45^\circ)} \begin{pmatrix} a_5^{(\mathrm{P})} \\ a_5^{(\mathrm{S})} \\ a_6^{(\mathrm{P})} \\ a_6^{(\mathrm{S})} \end{pmatrix}. \tag{49}$$

Similar equations follow for the other quarter wave plates, polarisers and the non-polarising beam splitter, leaving only the mirrors and photodiodes. Ideal mirrors may be modelled as previously discussed by setting the incident and excident beams to be equal, for example

$$\begin{pmatrix} b_7^{(\mathrm{P})} \\ b_7^{(\mathrm{S})} \end{pmatrix} = \begin{pmatrix} a_7^{(\mathrm{P})} \\ a_7^{(\mathrm{S})} \end{pmatrix} \tag{50}$$

for the reference mirror. The field component incident from the back surface of the photodiodes must be set to zero (or another known value) for the model to be solvable. Back reflections from the photodiodes could be modelled as a material interface if desired, although if the photodiodes are to be angled, as is common to avoid back reflections in experimental work, fixing the incident field at zero may produce more applicable results.

Each component must then be linked together. Some care is needed to ensure that the outputs and inputs to each component are coupled correctly when mixing transfer and scattering matrices; for scattering matrices the 'a' component is always the input, for transfer matrices this is only the case for one side of the stack of materials described by the transfer matrix. In practise this problem can be solved by ensuring all components are linked by transfer matrices, with no scattering matrix to scattering matrix connections, and then checking the directions of the field components linked to each end of the transfer stack. In this case the laser may be connected to the beam splitter with the transfer matrix equation

$$\begin{pmatrix} a_0^{(\mathrm{P})} \\ a_0^{(\mathrm{S})} \\ b_0^{(\mathrm{P})} \\ b_0^{(\mathrm{S})} \end{pmatrix} = \boldsymbol{M}_{0,1} \begin{pmatrix} a_1^{(\mathrm{P})} \\ a_1^{(\mathrm{S})} \\ b_1^{(\mathrm{P})} \\ b_1^{(\mathrm{S})} \end{pmatrix} \tag{51}$$

whereas the polarising beam splitter and reference arm quarter wave plate are linked by the equation

$$\begin{pmatrix} b_2^{(\mathrm{P})} \\ b_2^{(\mathrm{S})} \\ a_2^{(\mathrm{P})} \\ a_2^{(\mathrm{S})} \end{pmatrix} = \boldsymbol{M}_{2,5} \begin{pmatrix} a_5^{(\mathrm{P})} \\ a_5^{(\mathrm{S})} \\ b_5^{(\mathrm{P})} \\ b_5^{(\mathrm{S})} \end{pmatrix}. \tag{52}$$

Note that the order of the 'a' and 'b' components has been switched in the above equation.

Together, these scattering and matrix equations form a system of linear equations that may be written in the form of a single 88×88 network matrix equation,

$$\begin{pmatrix} 0 \\ \vdots \\ \vdots \\ \vdots \\ \vdots \\ 0 \\ a_0^{(\mathrm{P})} \\ a_0^{(\mathrm{S})} \end{pmatrix} = \boldsymbol{M}_{\mathrm{NET}} \begin{pmatrix} a_0^{(\mathrm{P})} \\ a_0^{(\mathrm{S})} \\ b_0^{(\mathrm{P})} \\ b_0^{(\mathrm{S})} \\ \vdots \\ a_{21}^{(\mathrm{P})} \\ a_{21}^{(\mathrm{S})} \\ b_{21}^{(\mathrm{P})} \\ b_{21}^{(\mathrm{S})} \end{pmatrix}. \tag{53}$$

For small systems it may be possible to find an analytical solution to this network equation, however in the vast majority of practical applications it is preferable to find a numerical solution. Numerical results for the system depicted in figure 3 are presented in the following section.

4 Results

Applying the previously described modelling methodology to the interferometer depicted in figure 3 results, in the ideal case with the polarisation axes of all components perfectly aligned and no unwanted back reflections present, in the outputs (for nodes 18 and 21) shown in figure 4. As expected, the model produces sinusoidal signals with a phase difference of 90°, resulting in a circular Lissajous.

Non-ideal behaviour may be introduced into the modelled signals by misaligning the waveplate in the PD2 output arm of the interferometer. Introducing a large rotational misalignment of 20° into the model results in the outputs shown in figure 5. This rotation of the output quarter wave plate introduces both an error in the phase difference between the output signals, and a reduction in the amplitude of the PD2 signal. Such effects would introduce errors if the interferometer outputs were to be used for displacement measurement [6].

So far, the results shown are identical to those that could have been reached through Jones matrix calculation, and show only sinusoidal errors (that is to say, errors that result in a distortion of the output signals to a different sinusoid) that could be corrected for in a displacement measuring interferometer with Heydemann style corrections [5], as implemented by Birch [6]. Of more interest with respect to the benefits of the proposed modelling approach are the effects of multiple reflections on the interferometer outputs, which in

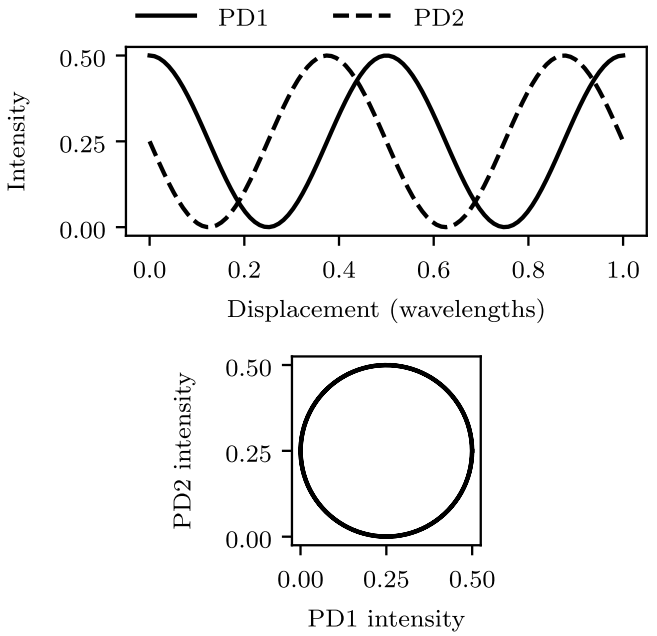

Figure 4: Ideal outputs of interferometer depicted in figure 3. Intensities are normalised to the input intensity.

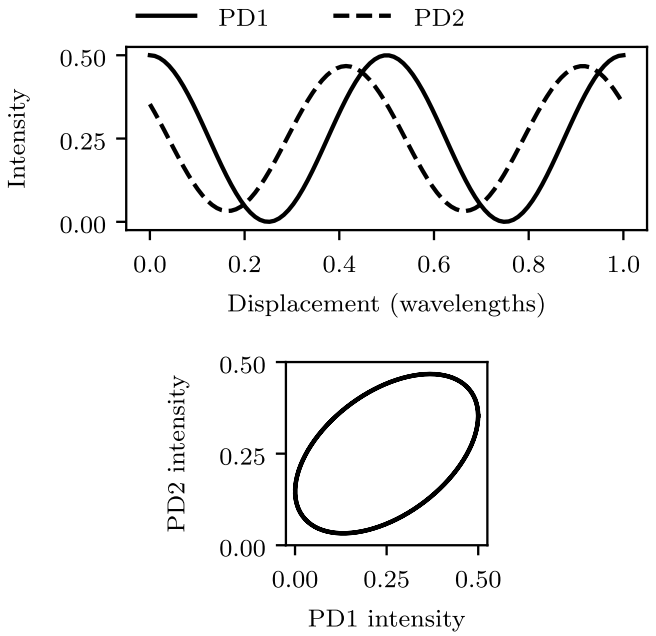

Figure 5: Outputs of interferometer depicted in figure 3 with the PD2 output quarter waveplate rotated by 20°. Intensities are relative to input intensity.

general result in the distortion of the output signals to a non-sinusoidal form. In general, finding an analytical form for the interferometer outputs with the presence of back reflections is challenging, indeed that is the problem that motivated the development of this model. In the simplified case of a cavity formed by the measurement mirror and another reflecting surface in the measurement arm of an otherwise ideal interferometer however, the analytical form is relatively simple and can be calculated for comparison with the modelled results. For an ideal polarising beam splitter and perfectly aligned waveplates, if a reflection at an air glass interface takes place between nodes 3 and 8 in figure 3, as may occur from the external surface of a polarising beam splitter cube, such that a cavity is formed by the beam splitter surface and M_{mes}, the amplitudes of the electric field components $b_4^{(\mathrm{P})}$ and $b_4^{(\mathrm{S})}$ are given by

$$b_4^{(\mathrm{P})} = A^{(\mathrm{S})} e^{ik2d_{ref}} \tag{54}$$

and

$$b_4^{(\mathrm{S})} = A^{(\mathrm{P})} t_{g\to a} t_{a\to g} \left(e^{ik2d_{mes}} + \sum_{n=0}^{\infty} r_{a\to g}^{2n+2} e^{ik(4n+6)d_{mes}} \right) \tag{55}$$

$$= A^{(\mathrm{P})} t_{g\to a} t_{a\to g} \left(e^{ik2d_{mes}} - \frac{r_{a\to g}^2 e^{ik6d_{mes}}}{r_{a\to g}^2 e^{ik4d_{mes}} - 1} \right) \tag{56}$$

where $A^{(\mathrm{S})}$ and $A^{(\mathrm{P})}$ are the S and P polarised amplitudes of the incident light, d_{ref} and d_{mes} are the lengths of the reference and measurement arms respectively, $r_{a\to g}$, $t_{g\to a}$ and $t_{a\to g}$ are the amplitude air to glass reflectivity, glass to air transmission and air to glass transmission coefficients, and k is the wavevector. The amplitude sum described in equation 56 results from only odd reflections from M_{mes} reaching node 4, as light having undertaken an even number of reflections from the mirror will be P polarised upon reaching the PBS, and therefore transmitted back towards the laser. From these amplitudes, the detected intensity at PD1 and PD2 may be calculated. If a refractive index of 1.515 is taken for the glass and 1 for the air, and the reference arm length is taken to be an exact multiple of the wavelength, equations 54 and 56 along with the model result in the signals shown in figure 6. The model produces the expected result in agreement with the exact analytical form given in equation 56, with the combination of the quarter waveplate and polarising beam splitter preventing alternate multiple reflections from reaching the detector. If such signals were to be used for displacement measurement, even if a Heydemann style correction were to be applied, errors in the measured displacement would still be present.

The non-circular nature of the Lissajous figure, and the presence of additional frequencies, can be more clearly seen in figure 7, where the refractive index of the glass has been increased to 3 to produce a particularly extreme example of the effects of back reflections. The results of a first order application of equation 55 are also shown in figure 7, the same result that would arise from applying a second order (the first order would be eliminated by the polarising beam splitter) Jones matrix model.

5 Discussion

The results presented here demonstrate that the described model produces the expected interferometer outputs when optical cavities are present within the optics. Whilst figure 7 shows a relatively good agreement between the model and

a first order Jones calculus based approximation, the utility of the modelling technique described here is in describing the behaviour of more complex networks consisting of many coupled cavities. If back reflections were added at all other optical surfaces in the interferometer depicted in figure 3 and polarisation leakage effects were included finding even the first order solution for each possible light path would be an extremely time consuming and error prone process. The model also allows the electric field at other points within the interferometer optics to be investigated without having to re-derive the possible beam paths, for example back reflections in the laser source. Another important point to note when considering multiple coupled cavities is that the relative phases of multiple light paths can have a significant effect on the resulting output. This can present a problem when considering macroscopic optical elements, as the exact spacing between surfaces may not be known. In this case the model can be used to find the maximum and minimum distortions to the desired ideal signals. Similar techniques can be used to identify the combined effect of polarisation aberrations arising from multiple optical components, where for example increasing the polarisation leakage of a polarising beam splitter may in fact improve interferometer performance by weakening cavities formed through the beam splitter.

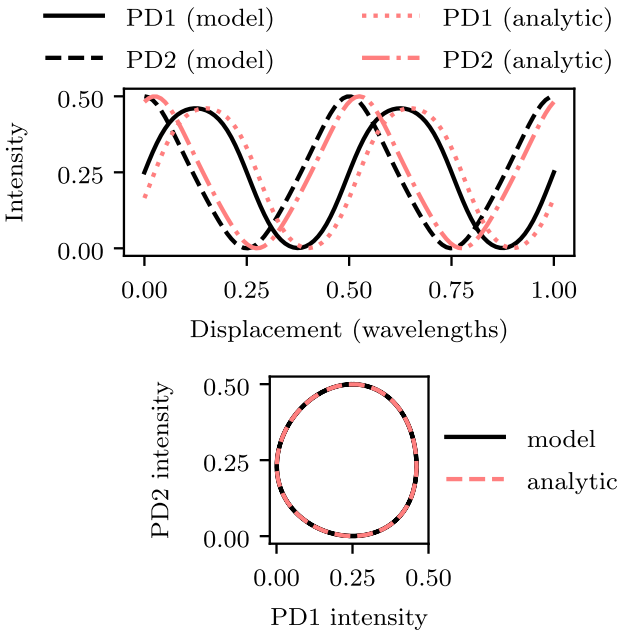

Figure 6: Outputs of interferometer depicted in figure 3 with a reflection for a glass-air interface between nodes 2 and 5, as calculated by both the described model and an exact analytical approach. A displacement offset has been added to the analytic signals in the left hand graph for clarity. Intensities are relative to input intensity.

The outputs of the model place an upper limit on the effects of multiple passes within the interferometer optics on the output signals; in reality the optical surfaces will not be perfectly aligned, and this misalignment will result in an attenuation of higher order multiple passes for finite diameter

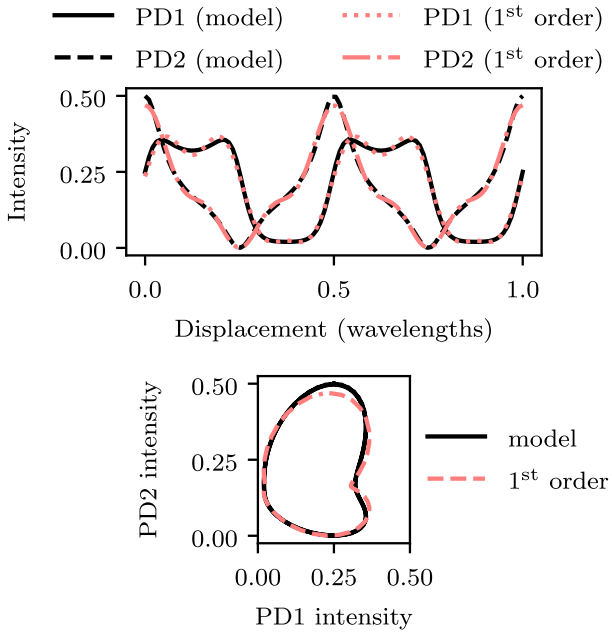

Figure 7: Outputs of interferometer depicted in figure 3 with a reflection for a glass-air interface between nodes 2 and 5, as calculated by both the described model and a first order analytical approximation. Intensities are relative to input intensity.

beams. Additional sources of round trip loss are likely to be present in real world interferometer designs, which could be included in this model. For example, the measurement mirror has been modelled as an ideal reflector here, it could however be modelled as an absorbing metallic mirror surface if desired. More complex cavity paths are likely to contain additional sources of loss, for example polarisation leakage from a non-ideal polarising beam splitter and reflections from material interfaces that have been wedged to prevent back reflections forming additional cavities. An important point to note is that ideal lossless cavities cannot be modelled, as such cavities will result in a singular network matrix. Singular network matrices can also be introduced by cavities containing components with optical gain. Whilst this is an unlikely case to be implemented intentionally, gain may be introduced by errors in the implementation of transmission through absorbing materials if sign conventions for complex refractive indices are not kept consistent.

The effects of birefringent optical components such as waveplates are currently modelled, a potential avenue for extension is the treatment of birefringent optics from first principles, integrating existing transfer matrix methodologies for anisotropic layers [32, 38, 39]. Although fundamentally a homodyne technique, there may be scope to model the outputs of heterodyne interferometers by considering the sum of the amplitude outputs of two or more homodyne interferometers.

This work focusses on the application of the described modelling technique to displacement measuring interferometers, however the method is widely applicable to any network of planar optical components. As such details of the results

of optical cavity formation within the optics of displacement measuring interferometers on the measured displacement have not been discussed, and may be presented in future work.

6 Conclusions

A modelling approach has been developed that permits the effects of multiple reflections though arbitrary networks of planar optical interfaces, including polarising components, to be modelled, extending prior comparable approaches, such as implemented in the FINESSE software, that cannot describe the effects of polarisation. Scattering or transfer matrices for a range of commonly used optical components have been described. The application of this modelling technique to a polarisation splitting homodyne interferometer has been demonstrated, and the agreement between the model and an exact analytical solution confirmed for the simple case of a cavity formed by a pair of optical surfaces within the measurement arm of an interferometer.

The modelling methodology presented here is well suited to computational implementation, and software has been developed [34] to automate the generation and solving of a network matrix equation from a list of optical components coupled at nodes. Modelling scripts to generate the figures presented in this paper are included in the software examples. Future work may describe the practical considerations in implementing this model, and describe how the software can be used to solve real world problems in the field of interferometry, along with potential extensions to model heterodyne designs.

Funding. Engineering and Physical Sciences Research Council Industrial CASE studentship EP/R511894/1 (Project 2199198); UK government Department for Business, Energy and Industrial Strategy, National Measurement System; Royal Academy of Engineering Research Fellowship RF\201718\1745.

Disclosures. The authors declare no conflicts of interest.

References

[1] Mise en pratique for the definition of the metre in the SI, Appendix 2 - SI Brochure. Consultative Committee for Length, Bureau international des poids et mesures, 9th edition, 2019.

[2] *The International System of Units*. Bureau international des poids et mesures, 9th edition, 2019.

[3] Richard K Leach, Robert Boyd, Theresa Burke, Hans-Ulrich Danzebrink, Kai Dirscherl, Thorsten Dziomba, Mark Gee, Ludger Koenders, Valérie Morazzani, Allan Pidduck, Debdulal Roy, Wolfgang E S Unger, and Andrew Yacoot. The European nanometrology landscape. *Nanotechnology*, 22(6):062001, 2011.

[4] Marco Pisani, Andrew Yacoot, Petr Balling, Nicola Bancone, Cengiz Birlikseven, Mehmet Çelik, Jens Flügge, Ramiz Hamid, Paul Köchert, Petr Kren, Ulrich Kuetgens, Antti Lassila, Gian Bartolo Picotto, Ersoy Şahin, Jeremias Seppä, Matthew Tedaldi, and Christoph Weichert. Comparison of the performance of the next generation of optical interferometers. *Metrologia*, 49(4):455–467, 2012.

[5] Peter L. M. Heydemann. Determination and correction of quadrature fringe measurement errors in interferometers. *Applied Optics*, 20(19):3382–3384, 1981.

[6] K. P. Birch. Optical fringe subdivision with nanometric accuracy. *Precision Engineering*, 12(4):195–198, 1990.

[7] Pengcheng Hu, Yue Wang, Haijin Fu, Jinghao Zhu, and Jiubin Tan. Nonlinearity error in homodyne interferometer caused by multi-order Doppler frequency shift ghost reflections. *Optics Express*, 25(4):3605, 2017.

[8] Andrew Yacoot and Michael J Downs. The use of x-ray interferometry to investigate the linearity of the NPL Interferometer. *Data Processing*, 11:1126–1130, 2000.

[9] Yasuaki Hori, Satoshi Gonda, Youichi Bitou, Akihiro Watanabe, and Koutaro Nakamura. Periodic error evaluation system for linear encoders using a homodyne laser interferometer with 10 picometer uncertainty. *Precision Engineering*, 51(July 2017):388–392, 2018.

[10] A. Bergamin, G. Cavagnero, and G. Mana. A displacement and angle interferometer with subatomic resolution. *Review of Scientific Instruments*, 64(11):3076–3081, 1993.

[11] H-J J. Büchner and G. Jäger. A novel plane mirror interferometer without using corner cube reflectors. *Measurement Science and Technology*, 17(4):746, 2006.

[12] Pengcheng Hu, Jinghao Zhu, Xiaoyu Zhai, and JiuBin Tan. DC-offset-free homodyne interferometer and its nonlinearity compensation. *Optics Express*, 23(7):8399, 2015.

[13] John Lawall and Ernest Kessler. Michelson interferometry with 10 pm accuracy. *Review of Scientific Instruments*, 71(7):2669–2676, 2000.

[14] S. Hosoe. Highly precise and stable laser displacement measurement interferometer with differential optical passes in practical use. *Nanotechnology*, 4(2):81–85, 1993.

[15] C Weichert, P Köchert, R Köning, J Flügge, B Andreas, U Kuetgens, and A Yacoot. A heterodyne interferometer with periodic nonlinearities smaller than ±10 pm. *Measurement Science and Technology*, 23(9):094005, 2012.

[16] Chien-ming Wu, John Lawall, and Richard D. Deslattes. Heterodyne interferometer with subatomic periodic nonlinearity. *Applied Optics*, 38(19):4089, 1999.

[17] Junning Cui, Zhangqiang He, Yuanwei Jiu, Jiubin Tan, and Tao Sun. Homodyne laser interferometer involving minimal quadrature phase error to obtain subnanometer nonlinearity. *Applied Optics*, 55(25):7086, 2016.

[18] J Liu and R M Azzam. Polarization properties of corner-cube retroreflectors: theory and experiment. *Applied optics*, 36(7):1553–9, 1997.

[19] R Clark Jones. A New Calculus for the Treatment of Optical Systems I . Description and Discussion of the Calculus. *Journal of the Optical Society of America*, 31(7):488–493, 1941.

[20] Henry Hurwitz and R. Clark Jones. A New Calculus for the Treatment of Optical Systems II. Proof of Three General Equivalence Theorems. *Journal of the Optical Society of America*, 31(7):493–499, 1941.

[21] R. Clark Jones. A New Calculus for the Treatment of Optical Systems III. The Sohncke Theory of Optical Activity. *Journal of the Optical Society of America*, 31(7):500–503, 1941.

[22] R. Clark Jones. A New Calculus for the Treatment of Optical Systems. IV. *Journal of the Optical Society of America*, 32(8):486–493, 1942.

[23] R. Clark Jones. A New Calculus for the Treatment of Optical Systems V. A More General Formulation, and Description of Another Calculus. *Journal of the Optical Society of America*, 37(2):107–110, 1947.

[24] R. Clark Jones. A New Calculus for the Treatment of Optical Systems VI. Experimental Determination of the Matrix. *Journal of the Optical Society of America*, 37(2):110–112, 1947.

[25] R. Clark Jones. A New Calculus for the Treatment of Optical Systems. VII. Properties of the N-Matrices. *Journal of the Optical Society of America*, 38(8):671–685, 1948.

[26] Daniel David Brown and Andreas Freise. FINESSE (http://www.gwoptics.org/finesse), 2014, accessed January 2019.

[27] A. Freise, G. Heinzel, H. Lück, R. Schilling, B. Willke, and K. Danzmann. Frequency-domain interferometer simulation with higher-order spatial modes. *Classical and Quantum Gravity*, 21(5), 2004.

[28] Gregory M. Harry. Advanced LIGO: The next generation of gravitational wave detectors. *Classical and Quantum Gravity*, 27(8), 2010.

[29] Pochi Yeh. Optical Waves in Layered Media. pages 62–63. John Wiley & Sons, Inc., Hoboken, New Jersey, 1998.

[30] Garam Yun, Karlton Crabtree, and Russell A. Chipman. Three-dimensional polarization ray-tracing calculus I: Definition and diattenuation. *Applied Optics*, 50(18):2855–2865, 2011.

[31] Garam Yun, Stephen C Mcclain, and Russell A Chipman. Three-dimensional polarization ray-tracing calculus II: retardance. *Applied Optics*, 50(18):2866–2874, 2011.

[32] Pochi Yeh. Electromagnetic propagation in birefringent layered media. *Journal of the Optical Society of America*, 69(5):742, 1979.

[33] Max Born and Emil Wolf. 1.6.2 The characteristic matrix of a stratified medium. In *Principles of Optics*, pages 51–71. Pergamon Press, Oxford, 6th edition, 1986.

[34] Angus Bridges, Andrew Yacoot, Thomas Kissinger, and Ralph P. Tatam. strapy - Scattering and TRAnsfer matrix model PYthon (10.17862/cranfield.rd.12001236, https://github.com/strapy-project/), 2020.

[35] G. Mana. Diffraction effects in optical interferometers illuminated by laser sources. *Metrologia*, 26(2):87–93, 1989.

[36] G Mana, E Massa, and C P Sasso. Wavefront errors in a two-beam interferometer. *Metrologia*, 55(4):535–540, 2018.

[37] Max Born and Emil Wolf. 7.3.3 Fringes with quasi-monochromatic and white light. In *Principles of Optics*, pages 264–265. Pergamon Press, Oxford, 6th edition, 1986.

[38] Pochi Yeh. Optics of anisotropic layered media: A new 4×4 matrix algebra. *Surface Science*, 96(1-3):41–53, 1980.

[39] Mathias Schubert. Polarization-dependent optical parameters of arbitrarily anisotropic homogeneous layered systems. *Physical Review B*, 53(8):4265–4274, 1996.

[40] Max Born and Emil Wolf. 1.5.2 Fresnel formulae. In *Principles of Optics*, pages 38–41. Pergamon Press, Oxford, 6th edition, 1986.

[41] Max Born and Emil Wolf. 13.2 Refraction and Reflection at a Metal Surface. In *Principles of Optics*, pages 615–624. Pergamon Press, Oxford, 6th edition, 1986.

https://dspace.org/

Polarization-sensitive transfer matrix modeling for displacement measuring interferometry

Bridges, Angus; Yacoot, Andrew; Kissinger, Thomas; Tatam, Ralph P.

2020-09-01
Optical Society of America
https://doi.org/10.1364/AO.396922
Bridges A, Yacoot A, Kissinger T, Tatam RP. (2020) Polarization-sensitive transfer matrix modelling for displacement measuring interferometry. Applied Optics, Volume 59, Issue 25, September 2020, pp. 7694-7704

Downloaded from a DSpace repository. https://dspace.org/